HHS Public Access

Author manuscript

J Mass Spectrom. Author manuscript; available in PMC 2016 July 01.

Published in final edited form as:

J Mass Spectrom. 2015 July ; 50(7): 891–898. doi:10.1002/jms.3597.

Laser Desorption Ionization of small molecules assisted by Tungsten oxide and Rhenium oxide particles

Matthew Bernier, **Vicki Wysocki**, and **Shai Dagan***

Ohio State University, Columbus Ohio

Abstract

Inorganic metal oxides have shown potential as matrices for assisting in laser desorption ionization (LDI) with advantages over the aromatic acids typically used. Rhenium and tungsten oxides are an attractive option due to their high work functions and relative chemical inertness. In this work, it is shown that ReO_3 and WO_3, in microparticle (μP) powder forms, can efficiently ionize various types of small molecules and provide minimized background contamination at analyte concentrations below 1 ng/μL. This study shows that untreated inorganic WO_3 and ReO_3 particles are valid matrix options for detection of protonatable, radical, and precharged species under LDI. Qualitatively, the WO_3 μP showed an improved detection of apigenin, sodiated glucose, and the precharged analyte choline, while the ReO_3 μP allowed detection of protonated cocaine, quinuclidine, ametryn, and radical ions of polyaromatic hydrocarbons at detection levels as low as 50 pg/μL. For thermometer ion survival yield experiments, it was also shown that the ReO_3 powder was significantly softer than CCA. Furthermore, it provided higher intensities of cocaine and polyaromatic hydrocarbons, at laser flux values equal to that used with CCA.

Introduction

One of the most robust and rapid mass spectrometry ionization techniques for large molecule analysis is matrix-assisted laser desorption ionization (MALDI). [1-3] This technique, developed in the work of Karas and Hillenkamp [4, 5] and Tanaka *et al.*[6], relies on the properties of matrix molecules coprecipitated on a plate with a target analyte, to absorb laser irradiation and subsequently desorb protonated molecules. Typically, the matrix is a small (100-300 Da) organic aromatic molecule with either proton donating or abstracting features. The conjugated aromatic property allows for efficient absorption of an incident UV laser beam to excite and transfer energy to the analyte. The process by which this occurs, however, is still under debate [7-12]. By having an acidic or basic character, the matrix is believed to assist in the protonation or deprotonation of analytes in either positive or negative mode mass spectrometry, respectively. When using this technique for smaller analytes, one major difficulty that arises is that, since the MALDI matrix is so abundant and a strong absorber of laser radiation, spectra can be plagued by matrix-derived interferences in the low mass range. This is true for many common matrices, such as 2, 4-dihydroxybenzoic acid (DHB), α-cyano-4-hydroxycinnaminic acid (CCA), and sinapinic acid, which exhibit protonated molecules at *m/z* 154, 189, and 224, respectively.

*Permanent Address: Israel Institute for Biological Research (IIBR), Ness-Ziona, Israel.

Furthermore, these matrices also produce proton-bound dimers, fragments, and other interfering matrix peaks in the LDI process.

Several techniques have been developed in recent years to eliminate complications in the low mass range, and produce high ionization efficiency of small target analytes without background peaks resulting from the chemical matrix. [13, 14] In lieu of standard organic matrices, many of these methods involve the use of inorganic substrates or particles so that there is no “contamination” of spectra by either a small molecule matrix or the inorganic substrate itself. One of the well-known techniques based on the use of inorganic substrates is desorption/ionization on porous silicon (DIOS), developed by Siuzdak *et al.*[15, 16]. In this process, the analyte is deposited onto a layer of porous silicon, which is generated *via* galvanostatic etching. The energy transferred to desorb the analyte is due to the UV absorption properties of the silicon wafer [16]. With this method small molecules, such as drugs and short peptides, can be detected at a femto/attomole level with highly reduced matrix-derived background in the mass spectra. Earlier work in surface-assisted laser desorption ionization (SALDI) utilized graphite as the surface and was applied to the analysis of small peptides, identifying several peptides from a tryptic digest, with no detrimental effects of matrix-derived interference in most cases. This technique was, however, limited by the production of carbon ion clusters at higher laser power irradiation [14, 17]. In recent years, silicon nanowire surfaces have been optimized as a commercial substrate under the name of nano-assisted laser desorption ionization (NALDI) [18-24]. Results have been promising for a wide array of analyte types and it has been proposed that NALDI is a more sensitive technique than other current alternative matrix LDI methods [20]. Additionally, Siuzdak and coworkers have recently developed a technique known as nanostructure initiator mass spectrometry.[25-28] This technique involved the use of etched silicon wafers with fluorinated and hydrocarbon polymeric “initiator” molecules co-imbedded in the Si nanostructures with the ions of interest.

Nano and microparticles have also been reported as a stage for producing small molecule laser desorption/ionization spectra with reduced matrix interference [20-36]. Previous work from our group in this area has focused on optimizing detection with 5-50 nm Si particles [29-31]. Like the porous surface used in DIOS, the level of background from nanoparticles of Si is low and an enhanced ionization effect can be observed. Low level detection of small drug molecules with almost no matrix peaks as interference has been readily achieved using this method. This technique, called SPALDI (silicon-nanoparticle-assisted laser desorption ionization) is part of a continuing effort to use inorganic nanoparticles for matrix free LDI of small molecule analytes. SPALDI, along with the other alternative, successful LDI techniques (NALDI, DIOS, NIMS), relies on the use of silicon as the main platform for ionization. In all of these techniques, however, chemical modification of the surface with a non-interacting species such as a perfluorinated compound is required to prevent oxidation and reduce the analyte-surface interactions that would suppress the analyte ion intensity in the mass spectra produced.

Other attempts have made use of metal oxides such as ZnO, MnO, CoO, WO_3, TiO_2, SnO_2, Fe_3O_4, CaO, NiO, and bare metals such as Au, Ag, Sn, and Al.[32-49] Clearly, the use of metal oxides as a base for laser desorption ionization has been investigated for several

compounds and the Vorhees' research lab, responsible for studies using CaO and NiO, have coined this work as "metal oxide laser ionization mass spectrometry" or MOLI-MS.[47-49]

In addition to the ability to efficiently absorb UV incident laser radiation and then transfer that energy to desorb and ionize a target analyte without any unintended ions formed, there are other characteristics of inorganic particles to consider that make them successful in assisting LDI of a target analyte. One of these is the interaction of the inorganic surface with the analyte molecules themselves; i.e. determining whether the LDI environment induces unintended interactions between the analyte and the particle/surface. This would be an issue with any metal oxide that can covalently bind to functional groups of an analyte or that may induce strong analyte-particle electrostatic forces, reducing the intensity of signal during laser irradiation.[50-52] Additionally, while the presence/transfer of protons is a necessity for many analyte molecules, the presence of strong electron donators or acceptors could also influence the ionization efficiency of small molecules, inducing electron transfers that could either enhance or decrease efficiency in the formation of cations and anions in an LDI environment.

In this work we focused specifically on the performance of several high work-function metal oxide particles, exploring their potential in matrix-assisted LDI of several small molecule analytes without any matrix signal interference. These included microparticle species of WO_3, WO_2, and ReO_3, in addition to nanoparticle size WO_3. In previous studies, the work-functions of Rhenium and Tungsten metals in oxygen-rich environments were found to be very high, in the range of 6.4 and 6.0 eV respectively [53, 54], and surfaces of those metals provided promising platforms for ionization due to these work-functions.[55, 56] These higher work-functions are also conducive to photodetachment. Tungsten oxide microstructured surfaces have previously been explored for LDI and seem to be able to promote ionization and enhancement of both protonation and electron transfer events. Rhenium oxide has been studied for its charge transfer properties while doped in layers of organic light-emitting diodes (OLEDs).[54, 57, 58] Using these metal oxide particles as bare metal surfaces for LDI, we expect an enhancement in positive mode ionization without the need for any modification step to passivate the surface. The analytes chosen in this work encompass a range of compounds and include compounds with varying affinities for protonation, precharged bio-related species, and molecules that could form radical ions via photodetachment. They included the readily protonatable drugs cocaine and ametryn, quinuclidine, the natural product apigenin, the relatively difficult to protonate sugar glucose, the precharged species choline, and a standard mixture of polyaromatic hydrocarbons described below, known to form radical ions upon laser desorption. Each metal oxide particle was compared to alpha-cyano-4-hydroxycinnamic acid (CCA) as a standard MALDI matrix, whose wide use and performance with protonatable small-molecule species is well documented.[59] Additionally, the fragmentation survival yields of 3-methyl benzylpyridine and cocaine were measured for all four matrices to assess the energy deposited upon LDI.

Experimental

WO_3 nanoparticles (nP) (< 100 nm), WO_3 microparticles (μP) (<20 μm), WO_2 μP (<150 μm), and ReO_3 powders were purchased from Sigma Aldrich. To make particle suspensions,

10 mg of each inorganic matrix was dispersed via sonication for approximately 60 minutes into 1 mL of nanopure H_2O purified in a Sartorius water purifier (18.3 Ω•cm). Standards of pure cocaine, ametryn, quinuclidine, apigenin, glucose, choline, and a polyaromatic hydrocarbon (PAH) standard mix were purchased from Sigma-Aldrich and each serially diluted to final concentrations of 1 ng/μL in MeOH for cocaine, 1 ng/μL in H_2O for ametryn and quinuclidine, 50 ng/μL apigenin in H_2O, 100 ng/μL glucose in H_2O, and 500 pg/μL of PAH standard. Some of these solutions were further diluted in H_2O to lower concentrations as noted below. To spot each sample, a 1:1 mixture of each inorganic particle solution and analyte solution was produced by mixing 4 μL of each and, after vortexing the suspension mixture, spotting 1 μL on a standard stainless steel MALDI plate.

The 3-methyl benzylpyridinium (BP) thermometer ions were synthesized using methods described previously.[30] 3-methyl benzylchloride and pyridine, purchased from Sigma-Aldrich (St. Louis, MO), were mixed together at a 1 to 1.2 equiv. ratio for 12 hours at room temperature in dry acetonitrile (Fischer Scientific). The resulting benzylpyridinium salt was crashed out of the ACN solution with the addition of cold diethyl ether, filtered, and then washed with hexane. Stock solutions of 1 mg/mL in nanopure H_2O were made from the solid salt and diluted to a concentration of 100 ng/μL in H_2O, for spotting onto the MALDI plate.

Spectra were collected on a Bruker “ultrafleXtreme” MALDI-MS operated in reflectron mode with a mass range set from m/z 20 to 900. This system uses a Smartbeam™ laser which combines both nitrogen and Nd: YAG technology to produce focused beams at 355 nm. The laser settings were maintained at a frequency of 20 Hz and in each run 500 shots were collected. The laser attenuator was set to an offset, or lower limit of half the full laser power, of 66 % with a range, or upper limit of 10% this value. Within this range, the percentages of 20 to 45 % were selectively scanned for all spectra in this work. Within this subrange of 20 to 45 % of the total laser flux, relative percentages of 20 to 45% were selected to produce all spectra.[flexControl 3.0 User Manual] The laser was manually rastered along the area of the spot, in each case, to sample for any potential hot spots and test whether the edge or middle of the spot was a better source of analyte ions.

Results

Ionization of small molecular ions with ReO_3 and WO_3 microparticles

Figure 1 and Figure 2 show collections of the low molecular weight analytes under LDI analysis with ReO_3 powder (Figure 1) and WO_3 μP (Figure 2) as the matrix. The four analytes of Figure 1, cocaine (Fig 1a), quinuclidine (Fig 1b), ametryn (Fig 1c), and a polyaromatic hydrocarbon standard mixture (Fig 1 d) exhibited the best LDI with ReO_3 μP compared to the other inorganic matrices (WO_3 nP, WO_3 μP, and WO_2 μP), as well as CCA and a “blank” spot (no matrix and only the stainless steel plate as a platform for LDI). Likewise, Figure 2 shows the three analytes that were ionized most efficiently by WO_3 μP: choline (Fig 2a), apigenin (Fig 2b), and glucose (Fig 2c). The criteria for selection included the overall intensity of the precursor at equivalent laser shots and flux, the suppression of background, the survivability of the precursor ion with respect to possible fragment ions in

the case of cocaine, and the ability to detect the widest range of analytes in the standard mixture of polyaromatic hydrocarbons.

In the case of the drug cocaine co-spotted with ReO_3 μP (Figure 1a), the dominant peak in the spectrum was the *m/z* 304.1 precursor, protonated *via* the single tertiary amine. At a concentration of 500 pg/μL, an additional distinct peak is observed at *m/z* 182, identified to be a cocaine fragment ion formed from the loss of benzoic acid, which has been commonly observed in both MALDI and ESI-MS investigations of cocaine.[60, 61] Both the precursor cocaine structure and the observed fragment are shown in the inset of the spectrum. The other two protonated analytes, quinuclidine and the pesticide ametryn, were also spotted with ReO_3 and, as with cocaine, no significant ReO_3 background was observed in these spectra (Figure 1b and 1c, respectively). Some background was, however, observed due to small impurities on the MALDI plate, which could be detected at lower concentrations of analyte. These impurities became more dominant as the analytes approached their limits of detection which for cocaine, was 5 pg/μL and that for quinuclidine and ametryn were slightly higher at 10 pg/μL.

In addition to the protonated analytes cocaine and ametryn, ReO_3 proved useful in detecting a mixture of polyaromatic hydrocarbons (PAHs), as shown in Figure 1c. The mixture was spotted at a concentration of 250 pg/μL. As each of the PAH analytes could directly absorb the laser and therefore not necessarily require any assistance in ionization, the concentration was lowered to determine the presence of chemical background with the inorganic particles studied. The four observed peaks at *m/z* 228, 252, 276, and 279 correspond to chrysene, benzo [k] fluoranthene, benzo [ghi] perylene, and dibenz [a,h] anthracene, respectively, with chrysene and benzo [ghi] perylene existing as radical ions.

ReO_3 provided a much cleaner signal than CCA and provided better detection of the lower mass peaks (*m/z* 228 and 252), as well as matched the signal of LDI with only water mixed 1:1 with the PAH standard solution (SI Figure 1). This demonstrates the advantage of ReO_3 to detect both protonated and self-ionizing radicals simultaneously, in mixtures, without any interference or matrix-derived ion suppression observed for a standard matrix, like CCA. As a matrix-free sample of only radical ions can be detected (SI Figure 1a), without background, so too can ReO_3. Additionally, ReO_3 can detect several other protonatable species with no background at low concentration (Figure 1) while a matrix-free spotting of these compounds would show no detection. Therefore, mixtures that contain both radically ionized species along with protonatable compounds should show simultaneous detection by using ReO_3 as the matrix. On the whole, ReO_3 μP provided the best LDI of the two protonated drugs as well as the radical ions of the PAH mixture. This may be due to the higher work-function of rhenium trioxide compared to other particles, where both radical and protonated ions would survive the laser desorption and energy transfer processes with little chance for neutralization on the particle surface via an electron transfer from, or proton transfer to the surface.

For the pre-charged quaternary amine choline, an essential nutrient, at *m/z* 104, WO_3 μP provided a strong and relatively isolated signal. Because choline does not require protonation, this analyte provided an interesting test for the nano and microparticle matrices.

Despite not outperforming CCA in the intensity of analyte (SI Figure 2), it did provide limited background interference, much lower than with the matrix derived peaks of CCA as well as a limit of detection of 100 pg/μL. Additionally, it may be argued that a matrix-free analysis of choline would result in strong LDI signal, because no protonation is required. However, SI Figure 2a shows the analyte spotted with water alone on the stainless steel plate and while this is a non-assisted LDI process, there is no *m/z* 104 signal observed in this spectrum, suggesting that analyte/surface interactions may hamper LDI of choline on the stainless steel.

The natural product apigenin, shown in Figure 2b, is an analyte that unlike those analytes observed in Figure 1, does not contain an amine group. For this reason, apigenin was more difficult to ionize than cocaine, ametryn, or quinuclidine and therefore required a higher concentration of 5 ng/μL for adequate signal-to-noise. At this concentration, a limited amount of background is observed at a relatively low intensity and does not appear to be matrix-derived. The LOD of apigenin was 250 pg/μL for WO3 μP and also showed a similar LOD of 300 pg/μL with higher and well isolated signal for ReO_3 as seen in SI Figure 3. In SI Figure 3a, ReO3 μP provides higher signal than WO3 μP, yet WO3 μP shows fewer impurities. In SI Figure 3c, CCA showed a signal several times higher than both ReO3 and WO3, but at this laser flux an overwhelming amount of matrix background interferences was present.

The analyte requiring the highest concentration on spot (50 ng/μL) was glucose as shown in Figure 2c. Glucose is a very difficult analyte to ionize, but was detected as the sodiated m/z 203 ion with minimal background with WO_3 μP as matrix. The signal at this concentration provided the cleanest spectrum but this analyte could even be detected as low as 1 ng/μL. Glucose is a difficult molecule to detect regardless of the ionization method chosen and its detection by WO_3 μP is likely due, in part, to the “edge” effect present for this matrix particle when spotted at a suspension concentration of 10 mg/mL. The “edge” effect (enhancement of analyte signal at the edge) is believed to be a spatial concentration of the analyte on the boundary of the spot as it moves with the solvent upon spotting, which results in an increased intensity of analyte at this area. This effect, however, did not appear to be a factor for the other three inorganic oxide particles. At the same analyte concentration, the other oxides tested produced a substantially weaker signal in comparison to that obtained with WO_3 microparticle, either on the edge or within the boundaries of the spot. Furthermore, sodium iodide was added to all the matrices to determine if a possible impurity of Na^+ was contributing to the elevated intensity of $[glucose+Na]^+$ for WO_3 μP. Interestingly, with the addition of this salt at 100 ng/μL, no improvement to the $[glucose+Na]^+$ signal was observed in any other matrix, while WO_3 μP still provided a clear m/z 203 peak.

Figure 3 presents lowered concentrations of cocaine (Fig 3a and 3b) and glucose (Fig 3c and 3d), at 50 pg/μL and 5 ng/ μL, respectively. The performances of ReO_3 μP for cocaine and WO_3 μP for glucose are compared to CCA at low concentrations where analyte detection is crucially dependent on minimization of background. This set of spectra highlights the promising ability of these metal oxides as matrices for providing small molecule signal with limited background interference derived from the matrix. In the case of cocaine, Figure 3a

CCA shows the m/z 304 precursor peak at less than 20% the relative base peak intensity, while five CCA matrix-derived peaks dominant the spectrum. The sensitivity distinctions between CCA and WO_3 μP for sodiated glucose in m/z 203 are even more pronounced, where, for a concentration of 5 ng/μL, the sodiated glucose peak is not even detectable for CCA, but for WO_3 μP, it is the most intense peak with very few background peaks and only one peak at m/z 158 reaching about 25 % relative intensity of the dominant sodiated glucose peak.

Survival yields of thermometer ions with each metal oxide matrices

In addition to the signal intensity and background, another interesting aspect of LDI is the amount of internal energy deposited into the analyte, reflecting on the "softness" of the LDI method. Results of the nano versus micro-size particles are discussed in more detail below with consideration of each particle's "softness" on both cocaine and the thermometer ion, 3-methyl benzylpyridinium (BP).

Apart from the ReO_3 μP and WO_3 μP results shown in Figure 1-3 WO_3 nP and WO_2 μP were also studied and Figure 4 summarizes the LDI survivability of the thermometer ions 3-methyl BP (Figure 4a and 4b) and cocaine (Figure 4c and 4d) for three particle types. The results with the WO_2 microparticle exhibited relatively high background and some instability upon increase of laser flux (not shown). This μP did not give improved results over standard CCA matrix, and therefore was not included in the thermometer ion comparison. Both cocaine and 3-methyl BP have an easily formed fragment ion and the relative ratio of the major fragment peak to the precursor was shown to vary significantly with the laser flux when either CCA or the three trioxide particles (ReO_3, WO_3 μP, WO_3 nP) were co-spotted. The survival yield (SY) is determined as the peak intensity ratio between the precursor and the (precursor + fragments) and can be used to determine the overall energy deposition for the ionization method being used. In the case of 3-methyl BP, the precursor at *m/z* 184 is fragmented by the loss of the neutral pyridine to form the *m/z* 105 fragment, where SY = I [184]/ (I [184] + I [105]) so that the higher the survival yield, the less fragmentation and the "softer" the resulting ionization of the sample being laser desorbed with the matrix. The same process was carried out for cocaine with the precursor at *m/z* 304 and major fragment at m/z 182, as shown in Figure 1a.

The matrices shown in Figure 4 include CCA in blue (diamonds), ReO_3 in red (squares), WO_3 μP (circles) in black, and WO_3 nP (triangles) in green. In Figure 4a, the survival yield breakdown of 3-methyl BP clearly demonstrates the "softest" ionization coming from ReO_3, with a small standard deviation between trials run on separate days. It is, however, evident that when the laser flux percentage was below 35%, SY with CCA improved dramatically and that below the lowest attenuation shown for both the 3-methyl BP (Figure 4a) and cocaine (Figure 4c), the CCA survival yield exceeds that of ReO_3. As laser flux increases, the SY with ReO_3 μP is retained and is higher than CCA, for both the pre-charged 3-methyl BP and the protonated cocaine analytes, even though in the case of cocaine the signal intensity is lower than with CCA.

Micro-sized versus nano-sized particle comparison

It is important to comment on the advantage of the WO_3 μP over the WO_3 nP. It might have been presumed that since the nanoparticle is <100 nm, it would absorb better in the region of the 355 nm wavelength and impart a greater amount of energy into the analytes, increasing the amount of LDI relative to the micro-sized particle. This is not the case, however, and throughout the 3-methyl BP and cocaine intensity plots (Figure 4 b and d, respectively), the WO_3 μP provide higher signal and better SY (i.e. "softer") for all cases, except for the 35% laser flux of 3-methyl BP, where the two are equivalent within error. Particle analysis with scanning electron microscopy (SEM) or transmission electron microscopy (TEM) was not performed to determine whether aggregation was a factor, resulting in the differences observed between the two particles. Whether it is the case that the 355 nm laser flux absorbance did not impart enough energy to overcome the advantage in crystallization and uniformity of the larger size particles or that the "edge" effect, where more analyte concentrated in the edge of the spot, could have been better facilitated by the greater space between particles of micro-particle size, is unclear. For the WO_3 μP and nP, the edge was a considerable factor in the concentration regions of the analytes. For ReO_3 it was less so but it also seemed to crystallize on the stainless steel plate, in a different way than the WO_3 compounds. While WO_3 formed tight, well defined circular spots with edges containing more of each compound, ReO_3 spots were more diffuse, as if the crystallization followed the path of the solution as it travelled left and right along the imperfections of the machined plate. More investigation is required to adequately determine the main cause for these observations and the differences in edge effects. It is, however, clear that there is a pronounced difference in "edge" effect between the smaller nano and larger micro-sized particles of WO_3 with a greater enhancement of signal for the micro-size and little advantage for nano.

Conclusions

It is the overall conclusion that two commercially available and stable metal oxides, ReO_3 and WO_3 μP, without any treatment but rather procured and spotted as is, can be used as LDI matrices for various applications, providing clean signal for trace amounts of analytes in the low mass range for specific classes of compounds as summarized in SI Table 1. Not only did the ReO_3 and WO_3 microparticles show clean and significant ionization for the analytes chosen, rhenium oxide either outperformed or matched CCA in intensity and survival yield of cocaine and 3-methyl BP at comparable laser flux, while tungsten oxide was able to detect sodiated glucose where no such peaks could be seen for CCA. The ReO_3 microparticle had a particular advantage over CCA at higher laser fluxes because even as laser flux increased, the inorganic particle was not observed to produce any matrix derived peaks cluttering the low mass regions, unlike CCA. It should be noted however, that in the case of lower laser fluence, CCA did provide higher signal than ReO_3, but always with more chemical noise.

In many cases in previous literature, particles used for assisting in LDI have required pretreatment with chemical modification, etching, or with the addition of proton sources to achieve the desired signal.[29, 30, 48] From experiments performed in direct comparison

with the high work-function particles in our lab, the lower work-function metals stainless steel (blank matrix) and untreated Fe_3O_4 (SI Figure 4) performed poorly. Only upon chemical modification, as has also been observed elsewhere in the literature [36], does iron oxide show even remotely comparable signal to the clean spectra observed for ReO_3 and WO_3. The clear advantage of these particles over other untreated compounds could be the result of a number of reasons and further mechanistic study is required to better understand this behavior. Additionally, having shown that a promising set of untreated particles are able to be utilized for a variety of analytes, future study could focus on the use of these compounds for biologically relevant compounds and metabolites, as per their ability to produce limited matrix derived background and the advantage of the apparent concentrating "edge" effect using WO_3.

Supplementary Material

Refer to Web version on PubMed Central for supplementary material.

Acknowledgements

The authors would like to thank Arpad Somogyi; Nanette Kleinholz; the University of Arizona Mass Spectrometry Facility in Tucson, AZ, USA; and the Campus Chemical Instrument Center (CCIC) Mass Spectrometry and Proteomics Facility at The Ohio State University, supported by NIH Award Number Grant 1 S10 RR025660-01A1.

References

1. Hillenkamp, F.; Jaskolla, TW.; Karas, M. The MALDI process and method. Wiley-VCH Verlag GmbH & Co. KGaA; 2014.
2. Kaufmann R. Matrix-Assisted Laser-Desorption Ionization (MALDI) Mass-Spectrometry - a Novel Analytical Tool in Molecular-Biology and Biotechnology. Journal of Biotechnology. 1995; 41(2-3): 155–175. [PubMed: 7654348]
3. Siuzdak G. The Emergence of Mass-Spectrometry in Biochemical-Research. Proceedings of the National Academy of Sciences of the United States of America. 1994; 91(24):11290–11297. [PubMed: 7972052]
4. Karas M, Hillenkamp F. Laser desorption ionization of proteins with molecular masses exceeding 10,000 daltons. Anal Chem. 1988; 60(20):2299–301. [PubMed: 3239801]
5. Stahl B, et al. Analysis of Neutral Oligosaccharides by Matrix-Assisted Laser Desorption - Ionization Mass-Spectrometry. Anal Chem. 1991; 63(14):1463–1466.
6. Tanaka K, et al. Protein and Polymer Analyses up to m/z 100,000 by Laser Ionization Time-of-flight Mass Spectrometry. Rapid Commun. Mass. Spectrom. 1988; 2(8):151–153.
7. Kruger R, et al. Analyte incorporation and ionization in matrix-assisted laser desorption/ionization visualized by pH indicator molecular probes. Analytical Chemistry. 2001; 73(24):5812–5821. [PubMed: 11791549]
8. Kruger R, Karas M. Formation and fate of ion pairs during MALDI analysis: Anion adduct generation as an indicative tool to determine ionization processes. Journal of the American Society for Mass Spectrometry. 2002; 13(10):1218–1226. [PubMed: 12387328]
9. Gabelica V, Schulz E, Karas M. Internal energy build-up in matrix-assisted laser desorption/ ionization. Journal of Mass Spectrometry. 2004; 39(6):579–593. [PubMed: 15236295]
10. Jaskolla TW, Karas M. Using fluorescence dyes as a tool for analyzing the MALDI process. Journal of the American Society for Mass Spectrometry. 2008; 19(8):1054–1061. [PubMed: 18513990]
11. Jaskolla TW, Karas M. Compelling Evidence for Lucky Survivor and Gas Phase Protonation: The Unified MALDI Analyte Protonation Mechanism. Journal of the American Society for Mass Spectrometry. 2011; 22(6):976–988. [PubMed: 21953039]

12. Soltwisch J, et al. Ion Yields in UV-MALDI Mass Spectrometry As a Function of Excitation Laser Wavelength and Optical and Physico-Chemical Properties of Classical and Halogen-Substituted MALDI Matrixes. Analytical Chemistry. 2012; 84(15):6567–6576. [PubMed: 22803742]
13. Silina YE, Volmer DA. Nanostructured solid substrates for efficient laser desorption/ionization mass spectrometry (LDI-MS) of low molecular weight compounds. Analyst. 2013; 138(23):7053–7065. [PubMed: 24133675]
14. Arakawa R, Kawasaki H. Functionalized Nanoparticles and Nanostructured Surfaces for Surface-Assisted Laser Desorption/Ionization Mass Spectrometry. Analytical Sciences. 2010; 26(12): 1229–1240. [PubMed: 21157090]
15. Wei J, Buriak JM, Siuzdak G. Desorption-ionization mass spectrometry on porous silicon. Nature. 1999; 399(6733):243–246. [PubMed: 10353246]
16. Shen ZX, et al. Porous silicon as a versatile platform for laser desorption/ionization mass spectrometry. Anal Chem. 2001; 73(3):612–619. [PubMed: 11217770]
17. Sunner J, Dratz E, Chen YC. Graphite Surface Assisted Laser Desorption/Ionization Time-of-Flight Mass-Spectrometry of Peptides and Proteins from Liquid Solutions. Analytical Chemistry. 1995; 67(23):4335–4342. [PubMed: 8633776]
18. Go EP, et al. Desorption/ionization on silicon nanowires. Analytical Chemistry. 2005; 77(6):1641–1646. [PubMed: 15762567]
19. Kang MJ, et al. Nanowire-assisted laser desorption and ionization mass spectrometry for quantitative analysis of small molecules. Rapid Communications in Mass Spectrometry. 2005; 19(21):3166–3170.
20. Shenar N, et al. Comparison of inert supports in laser desorption/ionization mass spectrometry of peptides: pencil lead, porous silica gel, DIOS-chip and NALDI (TM) target. Rapid Communications in Mass Spectrometry. 2009; 23(15):2371–2379. [PubMed: 19575411]
21. Guenin E, Lecouvey M, Hardouin J. Could a nano-assisted laser desorption/ionization target improve the study of small organic molecules by laser desorption/ionization time-of-flight mass spectrometry? Rapid Communications in Mass Spectrometry. 2009; 23(9):1395–1400. [PubMed: 19340850]
22. Vidova V, et al. Laser Desorption-Ionization of Lipid Transfers: Tissue Mass Spectrometry Imaging without MALDI Matrix. Analytical Chemistry. 2010; 82(12):4994–4997. [PubMed: 20491444]
23. Dupre M, et al. Silica nanoparticles pre-spotted onto target plate for laser desorption/ionization mass spectrometry analyses of peptides. Analytica Chimica Acta. 2012; 741:47–57. [PubMed: 22840704]
24. Yoshioka K, Ando D, Watanabe T. A Comparative Study of Matrix- and Nano-assisted Laser Desorption/Ionisation Time-of-Flight Mass Spectrometry of Isolated and Synthetic Lignin. Phytochemical Analysis. 2012; 23(3):248–253. [PubMed: 21898628]
25. Northen TR, et al. Clathrate nanostructures for mass spectrometry. Nature. 2007; 449(7165):1033–U3. [PubMed: 17960240]
26. Yanes O, et al. Nanostructure Initiator Mass Spectrometry: Tissue Imaging and Direct Biofluid Analysis. Analytical Chemistry. 2009; 81(8):2969–2975. [PubMed: 19301920]
27. Patti GJ, et al. Nanostructure-Initiator Mass Spectrometry (Nims) Imaging of Brain Cholesterol Metabolites in Smith-Lemli-Opitz Syndrome. Neuroscience. 2010; 170(3):858–864. [PubMed: 20670678]
28. Woo HK, et al. Nanostructure-initiator mass spectrometry: a protocol for preparing and applying NIMS surfaces for high-sensitivity mass analysis. Nature Protocols. 2008; 3(8):1341–1349. [PubMed: 18714302]
29. Wen XJ, Dagan S, Wysocki VH. Small-molecule analysis with silicon-nanoparticle-assisted laser desorption/ionization mass spectrometry. Analytical Chemistry. 2007; 79(2):434–444. [PubMed: 17222005]
30. Dagan S, et al. Internal energy deposition with silicon nanoparticle-assisted laser desorption/ionization (SPALDI) mass spectrometry. International Journal of Mass Spectrometry. 2009; 283(1-3):200–205.

31. Hua YM, et al. Analysis of deprotonated acids with silicon nanoparticle-assisted laser desorption/ionization mass spectrometry. Journal of Mass Spectrometry. 2010; 45(12):1394–1401. [PubMed: 21038364]
32. Schurenberg M, Dreisewerd K, Hillenkamp F. Laser desorption/ionization mass spectrometry of peptides and proteins with particle suspension matrixes. Analytical Chemistry. 1999; 71(1):221–229. [PubMed: 21662943]
33. Kinumi T, et al. Matrix-assisted laser desorption/ionization time-of-flight mass spectrometry using an inorganic particle matrix for small molecule analysis. Journal of Mass Spectrometry. 2000; 35(3):417–422. [PubMed: 10767772]
34. Yuan M, et al. Preparation of highly ordered mesoporous WO3–TiO2 as matrix in matrix-assisted laser desorption/ionization mass spectrometry. Microporous and Mesoporous Materials. 2005; 78(1):37–41.
35. Chen CT, Chen YC. Fe3O4/TiO2 core/shell nanoparticles as affinity probes for the analysis of phosphopeptides using TiO2 surface-assisted laser desorption/ionization mass spectrometry. Analytical Chemistry. 2005; 77(18):5912–5919. [PubMed: 16159121]
36. Chen WY, Chen YC. Affinity-based mass spectrometry using magnetic iron oxide particles as the matrix and concentrating probes for SALDI MS analysis of peptides and proteins. Analytical and Bioanalytical Chemistry. 2006; 386(3):699–704. [PubMed: 16685517]
37. McLean JA, Stumpo KA, Russell DH. Size-selected (2-10 nm) gold nanoparticles for matrix assisted laser desorption ionization of peptides. Journal of the American Chemical Society. 2005; 127(15):5304–5305. [PubMed: 15826152]
38. Huang YF, Chang HT. Nile red-adsorbed gold nanoparticle matrixes for determining aminothiols through surface-assisted laser desorption/ionization mass spectrometry. Analytical Chemistry. 2006; 78(5):1485–1493. [PubMed: 16503598]
39. Pan CS, et al. Recent developments in methods and technology for analysis of biological samples by MALDI-TOF-MS. Analytical and Bioanalytical Chemistry. 2007; 387(1):193–204. [PubMed: 17086385]
40. Su CL, Tseng WL. Gold nanoparticles as assisted matrix for determining neutral small carbohydrates through laser desorption/ionization time-of-flight mass spectrometry. Analytical Chemistry. 2007; 79(4):1626–1633. [PubMed: 17297965]
41. Sherrod SD, et al. Silver nanoparticles as selective ionization probes for analysis of olefins by mass spectrometry. Analytical Chemistry. 2008; 80(17):6796–6799. [PubMed: 18671412]
42. Lorkiewicz P, Yappert MC. Titania Microparticles and Nanoparticles as Matrixes for in Vitro and in Situ Analysis of Small Molecules by MALDI-MS. Analytical Chemistry. 2009; 81(16):6596–6603. [PubMed: 20337373]
43. Gholipour Y, et al. Diamond, Titanium Dioxide, Titanium Silicon Oxide, and Barium Strontium Titanium Oxide Nanoparticles as Matrixes for Direct Matrix-Assisted Laser Desorption/Ionization Mass Spectrometry Analysis of Carbohydrates in Plant Tissues. Analytical Chemistry. 2010; 82(13):5518–5526. [PubMed: 20518509]
44. Kailasa SK, Wu HF. Semiconductor cadmium sulphide nanoparticles as matrices for peptides and as co-matrices for the analysis of large proteins in matrix-assisted laser desorption/ionization reflectron and linear time-of-flight mass spectrometry. Rapid Communications in Mass Spectrometry. 2011; 25(2):271–280. [PubMed: 21192022]
45. Watanabe T, et al. Surface-assisted laser desorption/ionization mass spectrometry (SALDI-MS) of low molecular weight organic compounds and synthetic polymers using zinc oxide (ZnO) nanoparticles. Journal of Mass Spectrometry. 2008; 43(8):1063–1071. [PubMed: 18286665]
46. Walton BL, Verbeck GF. Soft-Landing Ion Mobility of Silver Clusters for Small-Molecule Matrix-Assisted Laser Desorption Ionization Mass Spectrometry and Imaging of Latent Fingerprints. Analytical Chemistry. 2014; 86(16):8114–8120. [PubMed: 25011014]
47. Voorhees KJ, McAlpin CR, Cox CR. Lipid profiling using catalytic pyrolysis/metal oxide laser ionization-mass spectrometry. J. Anal. Appl. Pyrolysis. 2012; 98:201–206.
48. McAlpin CR, Voorhees KJ. Extension of metal oxide laser ionization mass spectrometry to analytes with varied chemical functionalities. Rapid Commun. Mass Spectrom. 2013; 27(15):1763–1768. [PubMed: 23821569]

49. Voorhees KJ, et al. Modified MALDI MS fatty acid profiling for bacterial identification. J. Mass Spectrom. 2013; 48(7):850–855. [PubMed: 23832941]
50. Blesa MA, Regazzoni AE, Maroto AJG. Reactions of metal oxides with aqueous solutions. Mater. Sci. Forum. 1988; 29:31–97. (Copyright (C) 2014 American Chemical Society (ACS). All Rights Reserved.).
51. Truong TN, Johnson MA, Stefanovich EV. Electronic structure and chemical reactivity of metal oxides-water interfaces. ACS Symp. Ser. 2001; 789:124–141.
52. Dufour LC, et al. Fundamental and technological aspects of the surface properties and reactivity of some metal oxides. Solid State Ionics. 1997; 101:661–666.
53. Baikie ID, et al. Study of high- and low-work-function surfaces for hyperthermal surface ionization using an absolute Kelvin probe. Journal of Vacuum Science & Technology a-Vacuum Surfaces and Films. 2001; 19(4):1460–1466.
54. Yang XJ, et al. Microstructured Tungsten Oxide: A Generic Desorption/Ionization Substrate for Mass Spectrometry. Advanced Materials. 2010; 22(40):4520–4523. [PubMed: 20839246]
55. Dagan S, Danon A, Amirav A. Collisionally-Activated Dissociation in Hyperthermal Surface-Ionization of Cholesterol. International Journal of Mass Spectrometry and Ion Processes. 1992; 113(2):157–165.
56. Dagan S, Amirav A. High-Efficiency Surface-Induced Dissociation on a Rhenium Oxide Surface. Journal of the American Society for Mass Spectrometry. 1993; 4(11):869–873. [PubMed: 24227530]
57. Walter CW, et al. Photodetachment of WO3- - the Electron-Affinity of WO3. Journal of Chemical Physics. 1991; 95(2):824–827.
58. Luo JX, et al. ReOx charge injection/blocking layers in organic electronic devices. Journal of Physics D-Applied Physics. 2010; 43(38)
59. Zenobi R, Knochenmuss R. Ion formation in MALDI mass spectrometry. Mass Spectrometry Reviews. 1998; 17(5):337–366.
60. Jeanville PM, et al. Rapid confirmation/quantitation of cocaine and benzoylecgonine in urine utilizing high performance liquid chromatography and tandem mass spectrometry. J Am Soc Mass Spectrom. 2000; 11(3):257–63. [PubMed: 10697821]
61. Vogliardi S, et al. Validation of a fast screening method for the detection of cocaine in hair by MALDI-MS. Anal Bioanal Chem. 2010; 396(7):2435–40. [PubMed: 20063151]

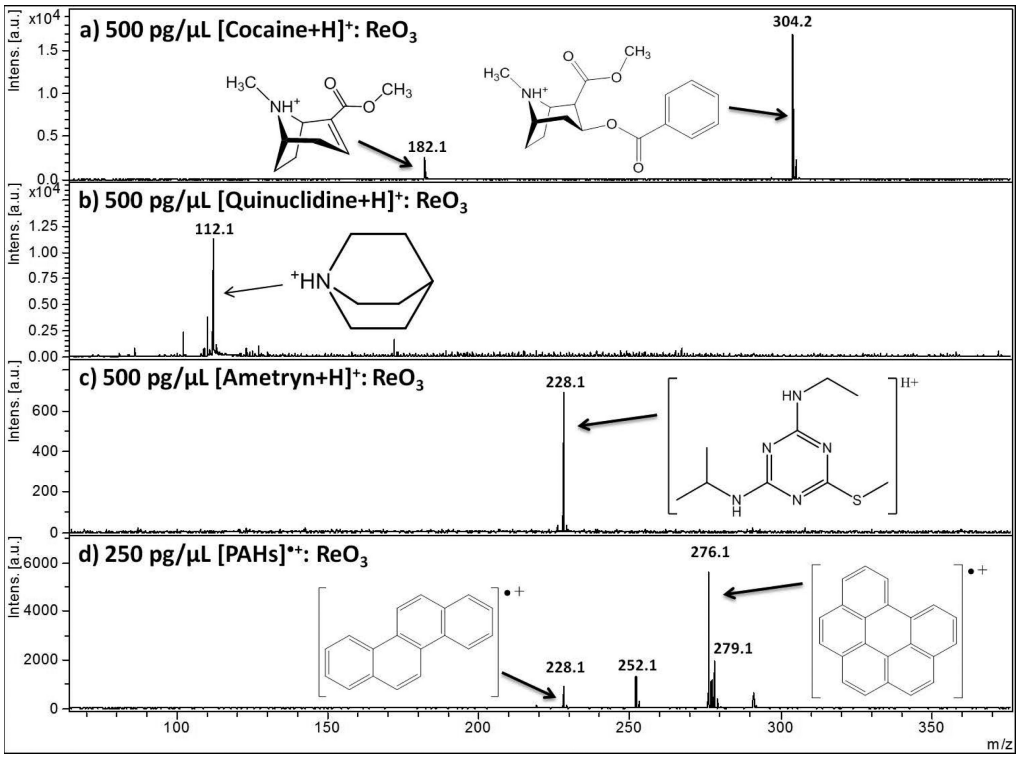

Figure 1.

Performance of a rhenium oxide powder, ReO3, as an assisting ionization material for small molecule analytes in positive LDI mode for a) 500 pg/µL protonated cocaine with its major fragment, b) 500 pg/µL protonated quinuclidine, c) 500 pg/µL protonated ametryn, and d) radical ions of a polyaromatic hydrocarbon (PAH) standard mixture with the four hydrocarbons chrysene (m/z 228), benzo [k] fluoranthene (m/z 252), benzo [ghi] perylene (m/z 276), and dibenz [a,h] anthracene (m/z 279) at 250 pg/µL each. Metal oxide particle suspensions were mixed 1:1 with each analyte (concentrations listed above after mixing) and 1 µL spotted on plate. Each case above provides the highest and cleanest signal among all particles explored with each analyte. 254×188mm (150 × 150 DPI)

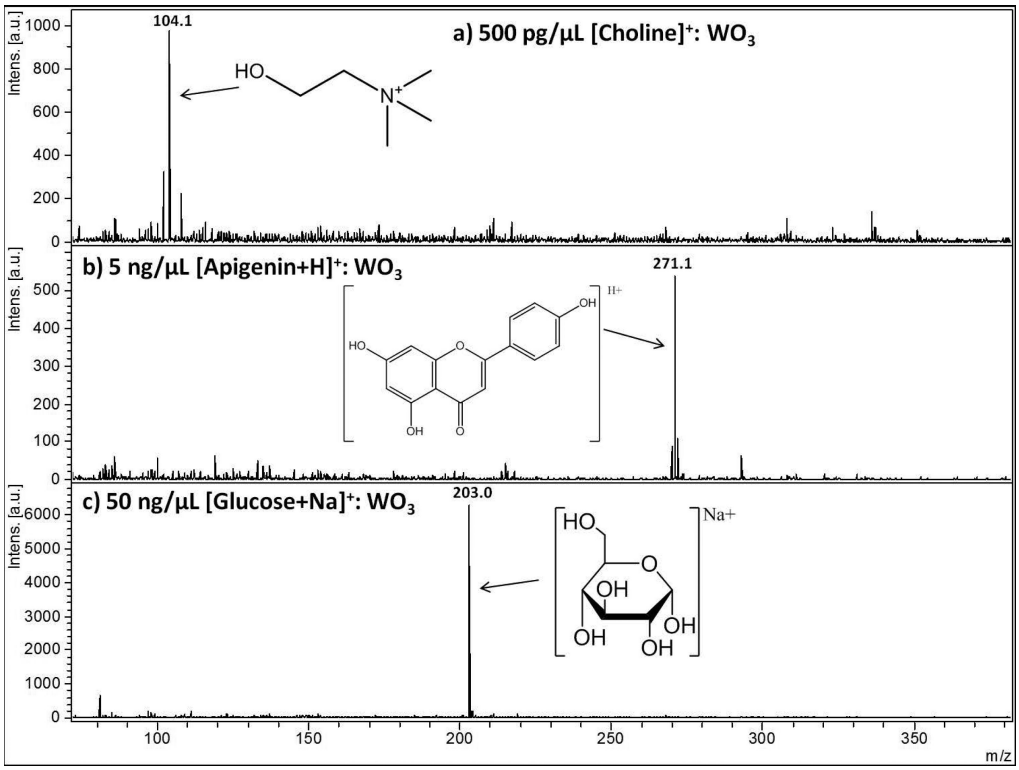

Figure 2.

Performance of a tungsten oxide micropowder, WO3, as an assisting ionization material for small molecule analytes in positive LDI mode for a) 500 pg/µL of the pre-charged choline analyte, b) 5 ng/µL protonated apigenin, and c) 50 ng/µL glucose with no additional source of sodium used. 254×191mm (150 × 150 DPI)

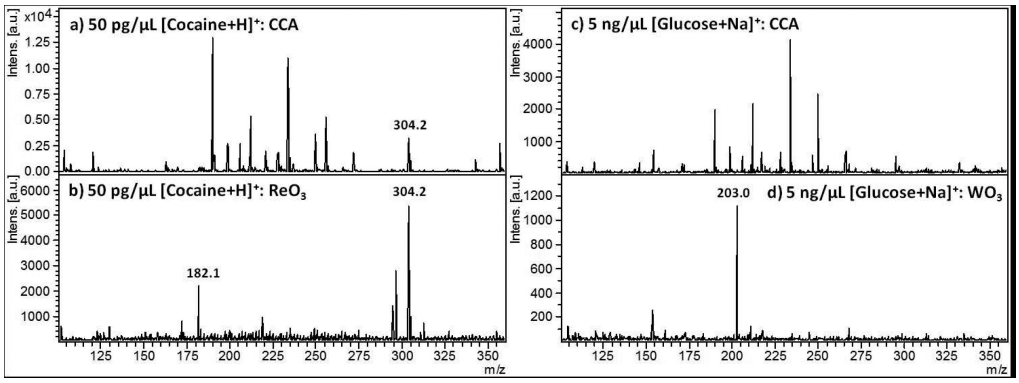

Figure 3.

Sensitivity of cocaine and glucose assisted by the ReO3 and WO3 µP laser desorption ionizations, versus MALDI using CCA: a) 50 pg/µL cocaine with CCA as matrix, b) 50 pg/µL cocaine with ReO3 as matrix, c) 5 ng/µL glucose with CCA as matrix, and d) 5 ng/µL glucose with WO3 µP as matrix. 252×92mm (150 × 150 DPI)

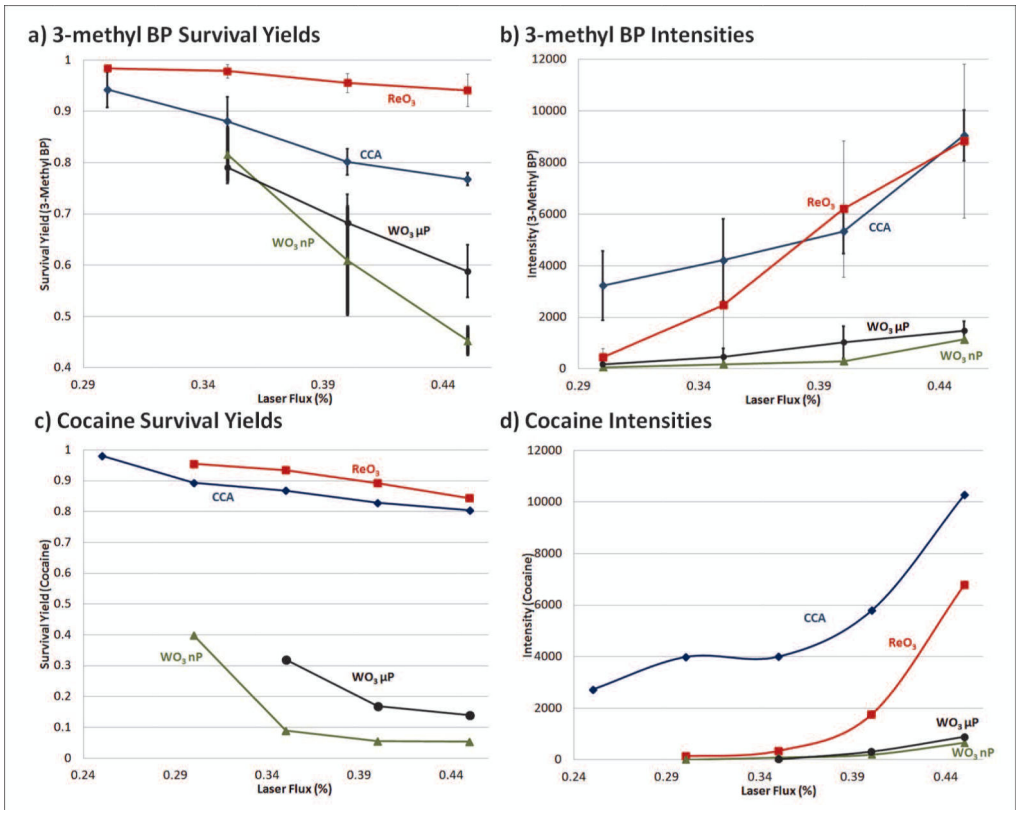

Figure 4.

Plots of survival yields versus laser flux percentage of a) 3-methyl BP ion at 50 ng/µL and for c) cocaine at 1 ng/µL for CCA matrix (blue diamonds), ReO3 µP (red squares), WO3 µP (black circles), and WO3 nP (green triangles). The overall intensity for 500 laser shots for b) 3-Methyl BP and d) cocaine are shown. In plots a) and b) error bars represent the standard deviation for an average of at least three runs taken at different days. 267×212mm (150 × 150 DPI)